Experimental analysis of small sample reactivity measured in the SEG experiment by a deterministic reactor physics code system CBZ

Go Chiba[1*] , Junshuang Fan[1]

[1] *Division of applied quantum science and engineering, faculty of engineering, Hokkaido University, Kita 13 Nishi 8, Kita-ku, Sapporo 060-8628, Japan*

Experimental analysis of the sample reactivity measured in the SEG experiment is carried out with the deterministic reactor physics code system CBZ with the recent evaluated nuclear data files, JENDL-4.0, ENDF/B-VIII.0 and JEFF-3.3.

Since the systems to be analysed are fast-thermal coupled ones, 211-energy group neutron reaction cross section libraries applicable to both the fast and thermal neutron systems are generated and utilized. In the multi-group library generation, the recently-developed FRENDY and FRENDY/MG codes are used. Forward and adjoint neutron fluxes at the sample position are calculated by solving the neutron transport equation, and the sample reactivity is obtained by the first-order perturbation calculations. In order to simplify the systems calculated, two-dimensional cylinder model is prepared based on the previous work.

Whereas the simplified model is employed, generally the reactivity of many different samples is well predicted by the calculations in comparison with the experimental uncertainties. On some of the samples, large discrepancies of the C/E values from unity are observed, and also relatively large differences in the C/E values among different nuclear data files are observed. These information are still useful for future development of the

evaluated nuclear data files.

Keywords: evaluated nuclear data files, integral data, benchmark calculations, sample reactivity

*Corresponding author. Email: go_chiba@eng.hokudai.ac.jp

1. Introduction

Nuclear data is one of the important fundamental data in the field of nuclear engineering. Significant efforts have been devoted to improve the accuracy and quality of the nuclear data since the accuracy of the nuclear data has large impact on the feasibility of the nuclear systems from the viewpoint of sustainability of nuclear fission chain reactions and radiation shielding. In order to achieve this, there are several approaches such as measurements of nuclear data itself or physical quantity directly related to specific nuclear data, and development of the sophisticated nuclear physics theory and model. Measurement of *integral parameters*, which are dependent on various nuclear data, are also important since the direct measurement of specific nuclear data is sometimes quite difficult. The measurement data on the integral parameters are also called *integral data*.

A lot of measurements on integral parameters have been conducted at various nuclear facilities all over the world so far. The detailed information of some of these data are gathered and summarised, and these information are released as benchmark problems which are easy to be utilized. These benchmark problems about the integral data are beneficial and useful to improve the nuclear data, and these have been efficiently utilized in the development of the recent evaluated nuclear data files.

One of the representative works of the benchmark problems about the integral data is a report compiled through the International Criticality Safety Benchmark Evaluation Project, the ICSBEP benchmark[1]. One feature of this benchmark is that a huge number of integral data, which are mainly on the neutron multiplication factor, are included. Since the neutron multiplication factor is defined from neutron production and disappearance rates over a whole system so that it is really an integral data, the contribution of nuclides, whose amount in the system are small, is generally less. Therefore, other kinds of integral parameters like neutron reaction rates and material reactivity are also useful for the nuclear data of such nuclides, and the measurement data of this kind of integral parameters

have been also acquired in nuclear facilities.

The small sample reactivity measured during the SEG experiment is one of the useful measurement data on integral parameters. This experiment was conducted to obtain information relevant to nuclear data of fission products, structural materials, and standards, and it was designed to obtain the integral data sensitive to neutron capture reactions or neutron scattering reactions. The acquisition of this kind of data was realized by changing the energy profile of the adjoint neutron flux at the measurement position, and this feature is specific to this experiment.

The information of the SEG experiment have been used in the nuclear data research in the past. One of the recent examples is the use in the benchmark calculations for the evaluated nuclear data file JENDL-4.0[2]. In the JENDL-4.0 development, revision was made for the lead isotopes, and their evaluation results were drastically changed from the previous one especially for the inelastic scattering cross sections. This had a large impact on the design calculations of the accelerator-driven system where lead is used as coolant[3], and validity of this revision was supported by the integral data of the SEG experiment[4]; the about 40% overestimation of the lead sample reactivity with the old file JENDL-3.3 has been resolved with JENDL-4.0. This is one good example clearly showing the usefulness of this integral data.

When conducting the analyses of the small sample reactivity of the SEG experiment, one needs to be careful about a fact that this nuclear system is a fast-thermal coupled system. Since the target quantity to be analysed is the small sample reactivity, the perturbation calculations based on the deterministic procedure are generally expected. In such cases, special cares should be taken to properly treat the fast-thermal coupled system since numerical calculations based on the deterministic procedure are historically conducted with the numerical tools dedicated to the specific type of reactors.

As mentioned above, the integral data obtained at the SEG experiment was used in

the JENDL-4.0 development, and a deterministic reactor physics code system CBZ[5] was utilized there. In this calculation, the spacial cares were taken to properly treat the fast-thermal coupled system, but its detail was not described in the paper about the JENDL-4.0 benchmarking[4]. In the present paper, the detail of the experimental analysis of the SEG experiment with CBZ is presented with numerical results using the recent evaluated nuclear data files, JENDL-4.0, ENDF/B-VIII.0[6] and JEFF-3.3[7]. In this experimental analysis, model simplification is made based on the previous work, and the detail of this simplified model is also presented.

In Section 2, the SEG experiment is briefly reviewed, and model simplification adopted in the present work is described in Section 3. The employed numerical methods and tools, and numerical results are presented in Section 4, and Section 5 is devoted to conclude the present study and to provide future perspective.

2. Brief description of the SEG experiment

The SEG experiment is well summarised in the report by Hummel[8]; thus this experiment is briefly reviewed here and interested readers can refer Hummel's report.

The abbreviation SEG stands for *Schnelles Einsatz-Gitter* in Germany, and it means a rapid (or fast) deployment lattice. The SEG lattice is composed of a cylindrical matrix of aluminium with a diameter of about 50 cm. It had cylindrical holes in the matrix, and these holes were filled with cylindrical pellets in defined order. The cylindrical hole configuration and the pellets arrangement are dependent on the lattices. The SEG lattice was introduced to the Rossendorf Research Reactor (RRR) in Germany, which was originally the Argonaut-type reactor having annular light water-moderated nuclear fuels surrounded by a graphite reflector. It also contained a removable internal graphite reflector, and this internal reflector was replaced by the SEG lattice. Since the SEG lattices included a small amount of neutron moderator and a large amount of thermal neutron absorbers like

boron and cadmium, neutron flux energy spectrum of a fast neutron reactor was formed in the SEG lattice. In the SEG lattice-introduced RRR cores (the SEG cores), the outer water-moderated nuclear fuel worked as a driver, and these cores were fast-thermal coupled systems. Between the internal SEG lattice and the outer driver region, a converter material, graphite or uranium, was placed.

The experimental setup with the SEG lattices at RRR was used to carry out the small sample reactivity measurements for fission products, structural materials, and standards. Several different versions of the SEG cores with different SEG lattices were constructed. In the present work, the cores with the SEG-4, -5, -6, and -7A lattices are treated since relevant information for these SEG cores are available for us. The cores with the SEG-6 lattices had two different versions with the different diameter of the experimental channel (EK) at the center of the cores, EK-10 and EK-45; thus the five cores in total, SEG-4, -5 -6/10, -6/45 and -7A, are treated in the present work.

The small sample reactivity was measured by the pile oscillator method. The samples to be measured were placed in special holders of graphite which moved through a window in the experimental channel. The dependence of the specific reactivity on sample size was determined for a wide mass range, and the extrapolation to infinitely diluted reactivity was performed. In the present work, we use the experimental data prepared by Dietze[9]. The uncertainties of the experimental data were also quantified by Dietze, and the following partial components were considered in his evaluation: statistical errors of the measurement with the sample and reference materials; errors of the extrapolation to infinitely diluted values of the sample and reference materials; errors caused by the deduction from molecular samples; data uncertainty of the reference materials; additional error dues to uncertainties in compositions and moisture.

These five SEG cores can be categorized into two according to the energy profile of the adjoint neutron flux at the sample position. The SEG-4, -5 and -7A cores were designed to

attempt to make energy dependence of the adjoint neutron flux negligibly small so that it could measure the sample reactivity induced by the neutron capture reaction. Generally the adjoint neutron flux level is increased as the neutron energy becomes low below several tens of keV, but this increase was suppressed by introducing the strong low-energy neutron absorbers such as boron (SEG-5 and -7A) or cadmium (SEG-4). Note that the polyethylene was also introduced to the SEG-7A lattice, and thus the SEG-7A core should have softer neutron flux than the SEG-5 core. Also, in high energy range above several tens of keV, the adjoint neutron flux level is increased as the neutron energy becomes high due to the uranium-238 threshold fission reaction and energy dependence of the averaged number of neutrons generated per a fission reaction, $\bar{\nu}$. This was also suppressed by using the relatively high uranium-235 concentration (around 36%) fuel. On the other hand, the SEG-6/10 and -6/45 cores had adjoint neutron flux which monotonically increases with the neutron energy. Under this condition, the scattering reactions in fast neutron energy range rather than the capture reactions become dominant to the sample reactivity. To achieve this, strong low-energy neutron absorber was introduced near the sample position, and the uranium-238 content was increased in comparison with the capture-dominant SEG cores.

Forward and adjoint neutron flux energy spectrum of the SEG cores will be presented in the following numerical calculation section.

3. Model simplification

Based on the previous work carried out by Dietze[9], we here propose a simple model specification for the small sample reactivity experiment with the SEG lattices at RRR.

The whole-reactor core is modelled as the cylindrical geometry as adopted in the previous work by Dietze. Region arrangement in the cylindrical core model is shown in **Figure 1**. Some of the region names are omitted in the right figure since these are same

as those in the left figure. The sample position is presented, but its composition is the same as the surrounding regions; "C" in SEG-4, -5 and -7A, and "Exchanger" in SEG-6. Radial and axial width of each region is shown in **Table 1**. The axial width is common for all the SEG core models. The region index corresponds to the numbers presented in Figure 1.

[Figure 1 about here.]

[Table 1 about here.]

The total volume of the driver region is determined so as to make these cores near critical in the calculations. Note that this volume setting has relatively large impacts on the reactivity of several samples in SEG-4, -5 and -7A. Most regions except for "Fuel" in SEG-4, -5 and -7A are treated as homogeneous media, and number density data for these media are shown in **Tables 2** and **3**. The region names in these tables correspond to those presented in Figure 1.

[Table 2 about here.]

[Table 3 about here.]

Only for the SEG lattices in SEG-4, -5 and -7A, one-dimensional slab heterogeneous cell model with the periodic boundary condition is prepared as done in the previous work. The unit cell model with width of each plate is shown in **Figure 2**.

[Figure 2 about here.]

Although the unit cell should be represented by a three-dimensional hexagonal lattice made of the aluminium matrix with the central hole where cylindrical pellets are stacked, these unit cells are modelled by the slab geometry in the present work. Hence all the plate regions include aluminium which is the matrix composition of the SEG lattices. The number density data of these plates are shown in **Table 4**.

[Table 4 about here.]

As mentioned above, the present work uses the experimental data with their uncer-

tainties prepared by Dietze, and hence no information is shown in the present paper. These can be referred in the reports by Dietze[9] and by Hummel[8]. The reaction-wise contribution to the total reactivity are also omitted here since it is almost the same as those presented in these existing reports[8, 9].

4. Numerical calculations and results

4.1. Numerical procedure and tool

In the present work, the conventional two-step method consisting of lattice calculation including spatial homogenization and whole-core calculation is adopted. All the calculations are carried out with a general-purpose reactor physics code system CBZ, which has been being under development at Hokkaido University.

The evaluated nuclear data files, JENDL-4.0, ENDF/B-VIII.0 and JEFF-3.3, are used in the present work. These data files are processed by the FRENDY code[10] to generate the ACE-formatted files including the probability tables for the unresolved resonance treatment, and then 211-energy group libraries are generated by the FRENDY/MG code[11]. Neutron slowing-down calculation capability of FRENDY/MG is used to calculate multi-group data in the resolved resonance range. The energy boundaries of this 211-group structure are same as those of VITAMIN-J above 1.85 eV and as those of the SRAC code below 1.85 eV in order to properly treat the fast-thermal coupled systems. The energy group structure of VITAMIN-J has been used in fast reactor core analyses[12], and that of SRAC has been used in thermal reactor core analyses[13]. Also, the thermal scattering data of carbon in graphite, hydrogen in polyethylene and hydrogen in water given in the respective evaluated nuclear data files are also processed with FRENDY and FRENDY/MG. Hence, the 211-group libraries consist of infinite dilution cross sections, scattering matrices, resonance self-shielding factors and thermal scattering cross section data.

With these 211-group libraries based on JENDL-4.0, ENDF/B-VIII.0 and JEFF-3.3, medium-wise 211-group macroscopic cross sections are calculated. For the one-dimensional heterogeneous cells, Tone's method[14] is used to calculate background cross sections of resonance nuclides considering the cell heterogeneity, and neutron flux spatial distributions, which are used as a weight in cross section spatial homogenization, are calculated with the collision probability method.

Finally, whole-core neutron transport calculations are conducted with a discrete-ordinate solver SNRZ of CBZ, and the reactivity of each sample is calculated based on the first-order perturbation theory using the forward and adjoint neutron fluxes at the sample position and infinite dilution 211-group cross sections of these samples. The first-order perturbation theory is appropriate since the experimental data of the sample reactivity are infinitely diluted. Note that the scattering anisotropy is considered by the first-order Legendre polynomial, and the S4 level symmetric quadrature set is used. The calculated reactivity is normalized by a weight of the corresponding sample calculated from an assumed number density, and C/E values are also normalized by that of the B-10 sample in SEG-4, -5 and -7A or that of the H-1 sample in SEG-6/10 and -6/45.

4.2. Numerical results

In order to help readers' understanding of the SEG experiment, forward and adjoint neutron fluxes at the sample position are calculated. Those for SEG-4, -5 and -7A are shown in **Figure 3**. Since these cores were devoted to the measurement of capture reaction-dominant reactivity, the adjoint neutron flux is almost flat with the neutron energy in the keV region. Among SEG-4, -5 and -7A, the hardest neutron flux spectrum is observed in SEG-5 as expected. The softest neutron flux energy spectrum is observed not in SEG-7A where polyethylene was introduced in the unit fuel cell, but in SEG-4. This is due to the relatively large amount of graphite in the unit cell in SEG-4. In SEG-7A, the

polyethylene plates were introduced in the unit cell, but the neutron moderation effect in the SEG-7A lattice was not as significant as the SEG-4 lattice. The product of forward and adjoint neutron fluxes at the sample position is shown in **Figure 4**. The group-wise reactivity effect is proportional to this quantity in capture-dominant reactivity, and this figure clearly shows that the data obtained at SEG-4 are the most sensitive to the low energy range among these three cores.

[Figure 3 about here.]

[Figure 4 about here.]

Forward and adjoint neutron fluxes at the sample position of SEG-6/10 and -6/45 are shown in **Figure 5**. The tail of neutron flux energy spectrum below 100 eV is not observed in both these cores because of the boron included in the sample exchanger region around the sample position. Steep gradient with the neutron energy in the adjoint neutron flux is also observed in these cores. Differences in the forward and adjoint neutron fluxes between these two cores are negligible.

[Figure 5 about here.]

The normalized C/E values of the sample reactivity obtained with the different three nuclear data files are shown in **Figures 6** to **10**. Generally good agreements are observed regardless of the evaluated nuclear data files, and differences among different nuclear data files are insignificant in comparison with the experimental uncertainties.

[Figure 6 about here.]

[Figure 7 about here.]

[Figure 8 about here.]

[Figure 9 about here.]

[Figure 10 about here.]

In some samples, large discrepancies of the C/E values from unity are observed, but sometimes inconsistency of the C/E values of the same sample among different cores is

observed. As an example, let us focus on the results of the Mo-100 sample. The Mo-100 sample reactivity is well predicted at SEG-5, but it is significantly underestimated at SEG-7A which has softer neutron spectrum than SEG-5. The underestimation is also observed at SEG-4, which has the softest neutron flux energy spectrum, but this underestimation is not as significant as that at SEG-7A. The same tendency was observed in the previous work by Hummel.[8] The energy group-wise Mo-100 sample reactivity, which is normalized so as to make total reactivity unity, is shown in **Figure 11**. The energy group profiles of the Mo-100 sample reactivity of the different cores are similar with each other, and it seems difficult to provide reasonable explanations on the significant underestimation observed only in the result at SEG-7A.

[Figure 11 about here.]

At SEG-6/10 and SEG-6/45, the sample reactivity of Al and Mg are overestimated by all the nuclear data files. To investigate this, normalized energy group-wise reactivities of the Al and Mg samples at SEG-6/45 are shown in **Figure 12**. Contributions of the elastic scattering, the inelastic scattering and the neutron capture to total reactivity are approximately 70%, 25% and 5% for all these samples; thus the elastic scattering reaction above 10 keV is dominant. Peaks observed in Figure 12 would correspond to resonance peaks of these nuclides. These results suggest that there is a possibility to improve nuclear data, especially the elastic scattering cross section, of Al-27 and Mg isotopes above 10 keV.

[Figure 12 about here.]

It is also interesting to point out that the Mn sample reactivity at SEG-6/45 is well predicted by JENDL-4.0 whereas the significant overestimations are observed in the same sample reactivity with ENDF/B-VIII.0 and JEFF-3.3. Contributions of the inelastic scattering and the elastic scattering to this sample reactivity are approximately 60% and 35%, respectively. Energy group-wise reactivity of this sample is shown in **Figure 13**. Large difference between JENDL-4.0 and the others is observed around several hundreds of

keV. This comes from a difference in the inelastic scattering cross section of Mn-55 in this energy range as shown in **Figure 14**, and the present result supports the JENDL-4.0 evaluation.

[Figure 13 about here.]

[Figure 14 about here.]

Large difference in C/E values is also observed in the V sample at SEG-6/45; while the JENDL-4.0 and ENDF/B-VIII.0 results show good agreement with the experimental value, JEFF-3.3 overestimates this sample reactivity. Energy group-wise reactivity of this sample is shown in **Figure 15**. Both of contributions of the elastic and inelastic scattering reactions to this reactivity are approximately 50%, and this integral data supports the JENDL-4.0 and ENDF/B-VIII.0 evaluation rather than the JEFF-3.3 evaluation on these cross sections. Comparisons of the elastic and inelastic scattering cross sections of V-51, which is dominant isotope in natural V, are shown in **Figure 16** and **Figure 17**. Note that the JENDL-4.0 evaluation and the ENDF/B-VIII.0 evaluation on the elastic scattering cross section are the same with each other below 100 keV since the same set of resonance parameters is adopted.

[Figure 15 about here.]

[Figure 16 about here.]

[Figure 17 about here.]

As described above, some of the measurement data of the sample reactivity of this experiment are still useful in future developments of evaluated nuclear data files.

5. Conclusion

Experimental analysis of the SEG experiment has been carried out with the deterministic reactor physics code system CBZ with the recent evaluated nuclear data files, JENDL-4.0, ENDF/B-VIII.0 and JEFF-3.3.

Since the systems to be analysed are fast-thermal coupled ones, 211-group cross section libraries applicable to both the fast and thermal neutron systems have been generated and utilized. In the multi-group library generation, the FRENDY and FRENDY/MG codes, which have been recently developed, have been used. The unit fuel cell heterogeneity has been taken into consideration at the cell calculation step, and medium-wise homogenized cross section data have been used in the whole-core calculation step. Forward and adjoint neutron fluxes at the sample position have been calculated by solving the neutron transport equation, and the sample reactivity has been obtained by the first-order perturbation calculations. In order to simplify the systems calculated, two-dimensional cylinder model has been prepared based on the previous work by Dietze.

Whereas the simplified model has been employed, generally the reactivity of many different samples has been well predicted by the calculations in comparison with the experimental uncertainties. On some of the samples, large discrepancies of the C/E values from unity have been observed, and also relatively large differences in the C/E values among different nuclear data files have been observed. These information would be still useful for future development of the evaluated nuclear data files.

The proposed calculation model for the SEG experiment would be useful also to test the advanced reactor physics code systems based on the deterministic procedure, such as APPOLO3[15], SARAX[16] and MC^2-3[17], which are applicable to reactors having the wide-range neutron energy spectrum.

The simplified model employed in the present work should have limitations due to relatively large uncertainties given to the experimental data. To further increase the usefulness of this measurement data, the construction of the detailed as-built numerical model would be necessary to reduce the experimental uncertainties although such works with the old literatures should be quite hard. When the as-built numerical model is available, it would be challenging and interesting to tackle with the advanced deterministic codes

since detailed spatial modelling is required. Also the Monte-Carlo perturbation capability as attempted by Hummel[8] would be useful and is strongly desired.

References

[1] Briggs JB. Ed. International Handbook of Evaluated Critical Safety Benchmark Experiments. France: OECD, Nuclear Energy Agency; 2010, NEA/NSC/DOC(95)03.

[2] Shibata K, Iwamoto O, Nakagawa T, et al. JENDL-4.0: A new library for nuclear science and technology. J Nucl Sci Technol. 2011; 48:1-30.

[3] Iwamoto H, Nishihara K, Tsujimoto K, et al. Analysis of transmutation systems using JENDL-4.0. JAEA-Research 2011-036; Japan Atomic Energy Agency; 2011. [in Japanese]

[4] Chiba G, Okumura K, Sugino K, Nagaya Y, Yokoyama K, Kogo T, Ishikawa M, Okajima S. JENDL-4.0 benchmarking for fission reactor applications. J Nucl Sci Technol. 2011; 48:172-187.

[5] Chiba G, Endo T. Numerical benchmark problem of solid-moderated enriched-U-loaded core at Kyoto university critical assembly. J Nucl Sci Technol. 2019; 57:187-195.

[6] Brown DA, Chadwick BM, Capote R, et al. ENDF/B-VIII.0: The 8th major release of the nuclear reaction data library with CIELO-project cross sections, new standard and thermal scattering data. Nucl. Data Sheets. 2018; 148;1-142.

[7] Plompen A, Cabellos O, Saint Jean C, et al. The joint evaluated fission and fusion nuclear data library, JEFF-3.3. The European Physical Journal A. 2020;56:181.

[8] Hummel A, Palmiotti G. Small sample reactivity measurements in the RRR/SEG facility: reanalysis using TRIPOLI-4. INL/EXT-16-39582; Idaho National Laboratory; 2016.

[9] Dietze K. Analysis of the Rossendorf SEG experiments using the JNC route for reactor calculation. JNC TN9400 99-089; Japan Nuclear Fuel Cycle Development Institute; 1999.

[10] Tada K, Nagaya Y, Kunieda S, Suyama K, Fukahori T. Development and verification of a new nuclear data processing system FRENDY. J Nucl Sci Technol. 2017; 54:806-817.

[11] Yamamoto A, Tada K, Chiba G, Endo T. Multi-group neutron cross section generation capability

for FRENDY nuclear data processing code. J Nucl Sci Technol.

[12] Hazama T, Chiba G, Sugino K. Development of a fine and ultra-fine group cell calculation code SLAROM-UF for fast reactor analyses. J Nucl Sci Technol. 2006; 43;908-918.

[13] Okumura K, Kugo T, Kaneko K, Tsuchihashi K. SRAC2006: a comporehensive neutronics calculation code system. JAEA-Data/Code 2007-004; Japan Atomic Energy Agency; 2007.

[14] Tone T. Space-dependent neutron spectrum effects in a fast reactor. J Nucl Sci Technol. 1975; 12:190-193.

[15] Schneider D, Dolci F, Gabriel F, et al. APOLLO3: CEA/DEN deterministic multi-purpose code for reactor physics analysis. Proc. Int. Conf. Physics of Reactors, PHYSOR2016; 2016 May 1-5; Sun Valley, Idaho.

[16] Wei L, Zheng Y, Du X, et al. Extension of SARAX code system for reactors with intermediate spectrum. Nucl. Eng. Design. 2020; 370; 110883.

[17] Lee CH. Yang WS. MC^2-3: multigroup cross section generation code for fast reactor analysis. Nucl. Sci. Eng. 2017; 187; 268-290.

Table 1 Radial and axial width of regions (unit: cm)

Region	Radial width				Axial width
index	4, 5	7A	6/10	6/45	Common
1	0.5	0.5	0.5	0.5	0.05
2	1.75	1.75	0.1	2.0	8.0
3	17.75	17.75	0.2	0.15	19.85
4	3.85	3.85	5.75	3.9	31.0
5	6.15	6.15	0.2	0.2	2.0
6	8.0	7.7	4.57	4.57	31.0
7	7.0	7.3	7.93	7.93	3.0
8	45.3	45.3	4.45	4.45	20.15
9			6.16	6.16	
10			8.8	8.8	
11			7.31	7.31	
12			45.0	45.0	

Table 2 Number density data of homogeneous regions (non-fuel, unit: [/cm^2/barn])

Region name	C	Cd	Al	H-1	O-16	B-10	B-11
C	8.030e-2						
Al			6.030e-2				
Cd		4.640e-2					
H_2O				6.660e-2	3.330e-2		
Al+C	7.741e-2		2.179e-3				
Polyethylene	3.851e-2			7.703e-2			
Exchanger (6/10)	2.190e-2					1.797e-2	6.966e-2
Exchanger (6/45)	2.190e-2					1.598e-2	6.196e-2
ABS (6/10)	1.614e-2					1.324e-2	5.133e-2
ABS (6/45)	1.603e-2					1.315e-2	5.098e-2

Table 3 Number density data of homogeneous regions (fuel, unit: [/cm^2/barn])

Region name	U-235	U-238	C	Al	H-1	O-16
U	3.210e-4	4.545e-2				
U5	1.215e-2	2.155e-2		1.594e-2		
U8	2.300e-4	3.304e-2		1.645e-2		
Thermal driver (4, 6, 7A)	1.480e-4	5.850e-4	6.585e-3	1.816e-2	3.274e-2	2.059e-2
Thermal driver (5)	1.200e-4	4.810e-4	2.177e-2	3.198e-3	3.104e-2	1.772e-2

Table 4 Number density data of plates in the unit cells (unit: [/cm^2/barn])

Plate name	U-235	U-238	C	Cd	Al	H-1	B-10	B-11
U	1.281e-2	2.271e-2			1.285e-2			
C			6.222e-2		1.285e-2			
C+B			6.727e-2		1.711e-2		9.745e-4	3.787e-3
Cd				3.693e-2	1.285e-2			
Poly			3.066e-2		1.285e-2	6.133e-2		

Figure Captions

Figure 1 Cylindrical whole-core model of the SEG cores

Figure 2 Unit cell configuration

Figure 3 Forward and adjoint neutron fluxes at the sample position of SEG-4, -5 and -7A

Figure 4 Product of forward and adjoint neutron fluxes (bilinear flux) at the sample position of SEG-4, -5 and -7A

Figure 5 Forward and adjoint neutron fluxes at the sample position of SEG-6/10 and -6/45

Figure 6 Normalized C/E values of the sample reactivity at SEG-4 with the recent nuclear data files

Figure 7 Normalized C/E values of the sample reactivity at SEG-5 with the recent nuclear data files

Figure 8 Normalized C/E values of the sample reactivity at SEG-6/10 with the recent nuclear data files

Figure 9 Normalized C/E values of the sample reactivity at SEG-6/45 with the recent nuclear data files

Figure 10 Normalized C/E values of the sample reactivity at SEG-7A with the recent nuclear data files

Figure 11 Energy break-down of the Mo-100 sample reactivity

Figure 12 Energy break-down of the Al and Mg sample reactivity at SEG-6/45

Figure 13 Energy break-down of the Mn sample reactivity at SEG-6/45

Figure 14 Inelastic scattering cross section of Mn-55

Figure 15 Energy break-down of the V sample reactivity at SEG-6/45

Figure 16 Elastic scattering cross section of V-51

Figure 17 Inelastic scattering cross section of V-51

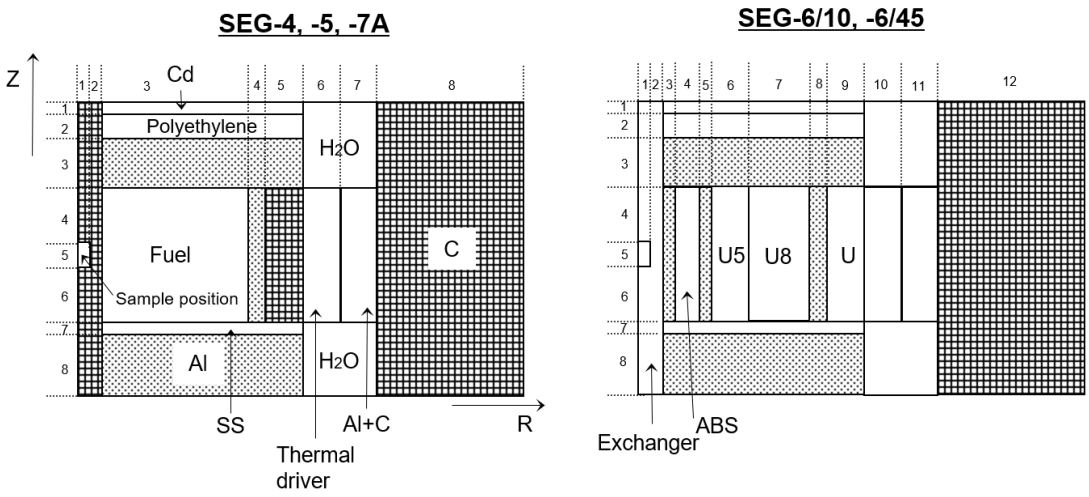

Figure 1 Cylindrical whole-core model of the SEG cores

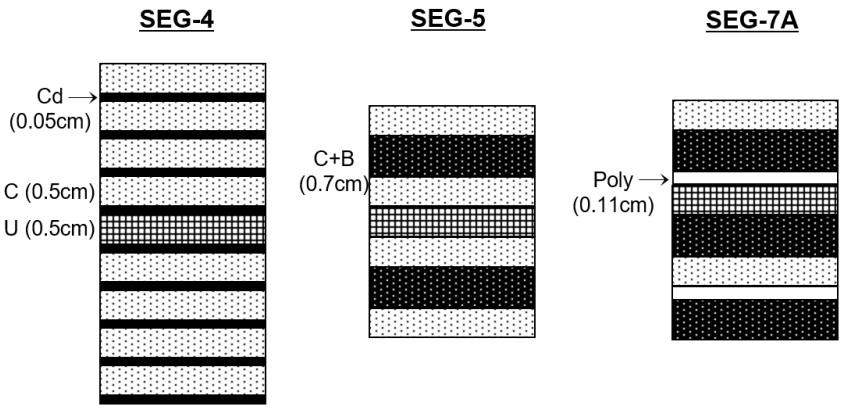

Figure 2 Unit cell configuration

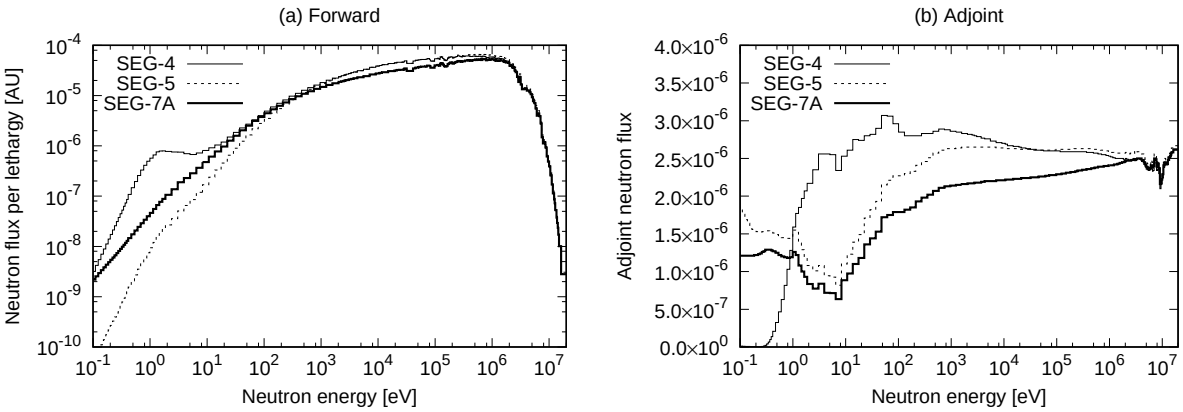

Figure 3 Forward and adjoint neutron fluxes at the sample position of SEG-4, -5 and -7A

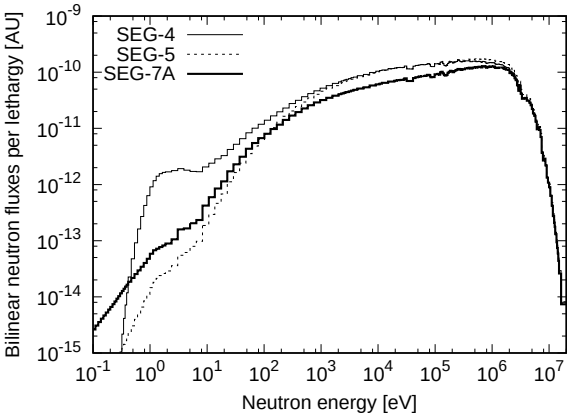

Figure 4 Product of forward and adjoint neutron fluxes (bilinear flux) at the sample position of SEG-4, -5 and -7A

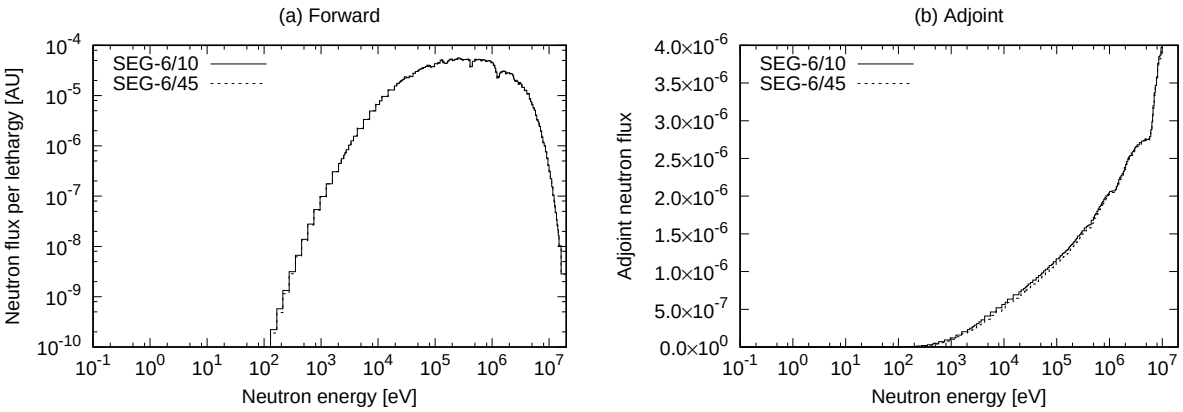

Figure 5 Forward and adjoint neutron fluxes at the sample position of SEG-6/10 and -6/45

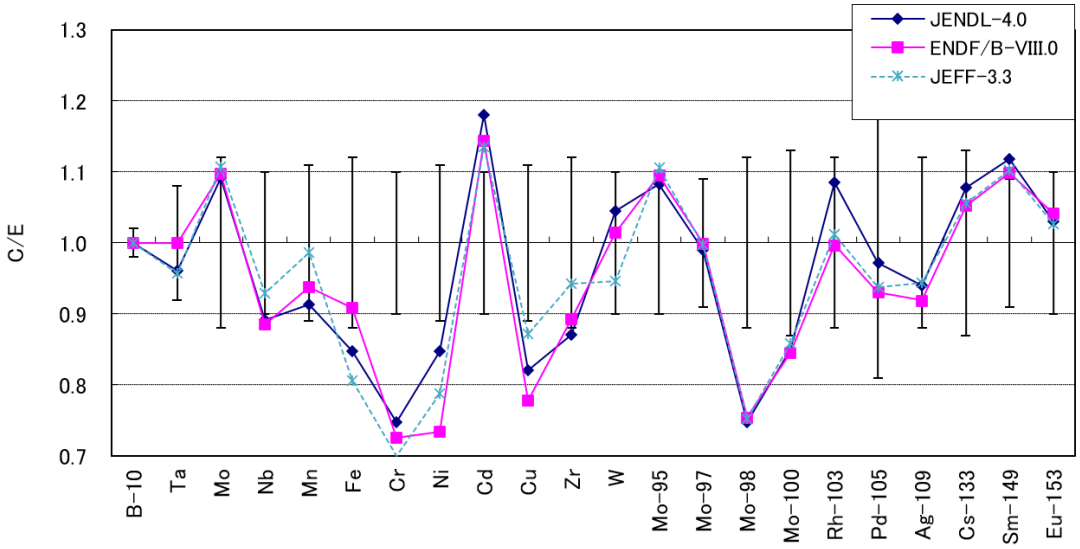

Figure 6 Normalized C/E values of the sample reactivity at SEG-4 with the recent nuclear data files

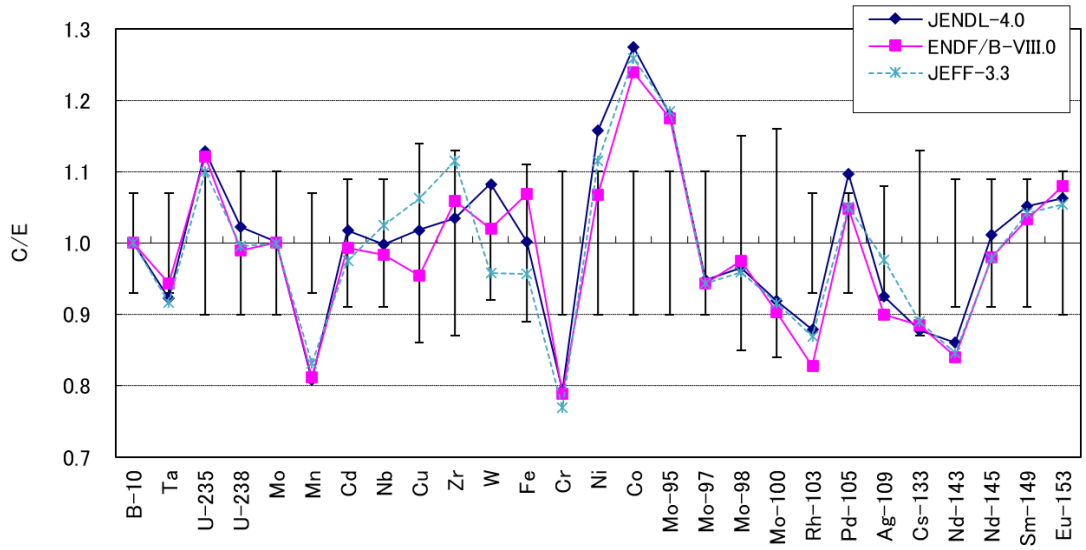

Figure 7 Normalized C/E values of the sample reactivity at SEG-5 with the recent nuclear data files

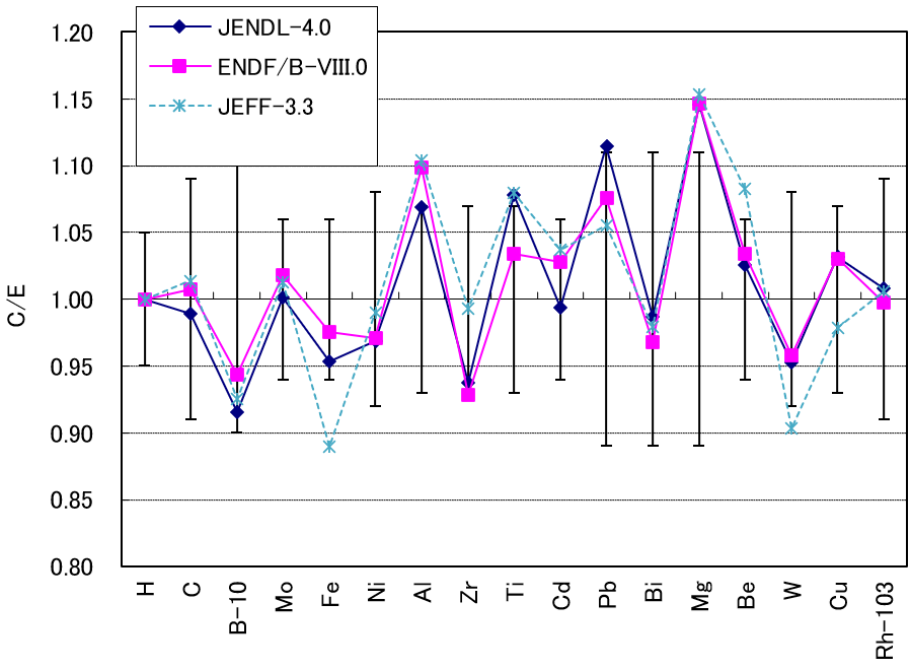

Figure 8 Normalized C/E values of the sample reactivity at SEG-6/10 with the recent nuclear data files

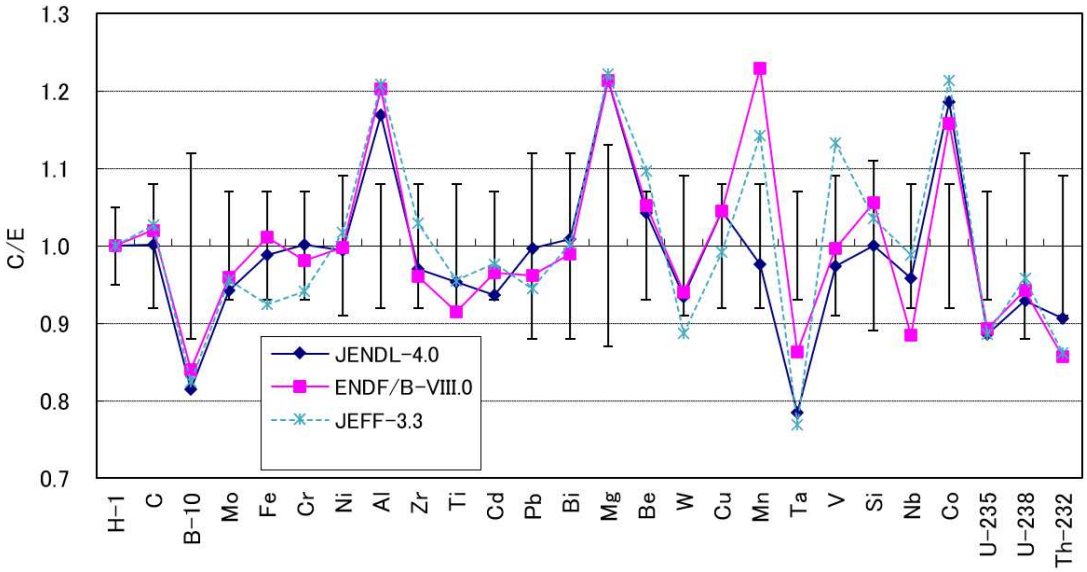

Figure 9 Normalized C/E values of the sample reactivity at SEG-6/45 with the recent nuclear data files

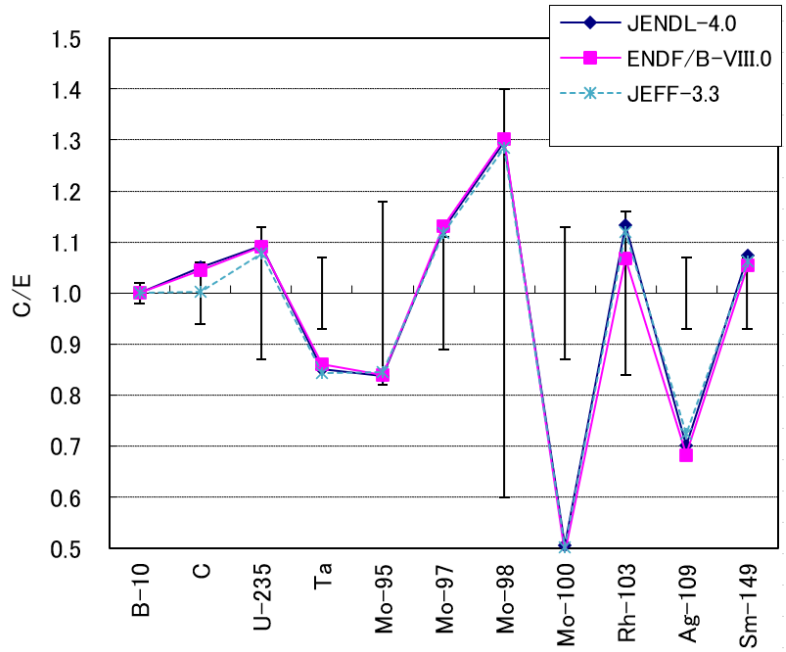

Figure 10 Normalized C/E values of the sample reactivity at SEG-7A with the recent nuclear data files

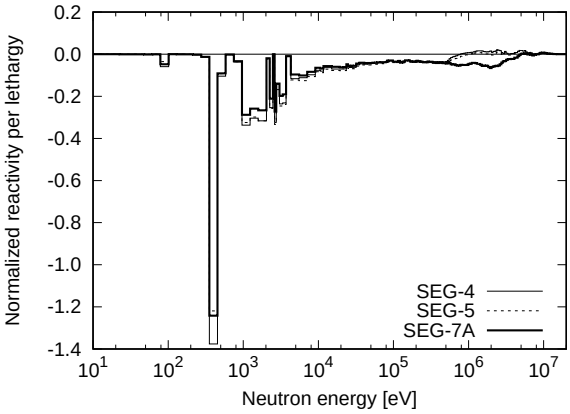

Figure 11 Energy break-down of the Mo-100 sample reactivity

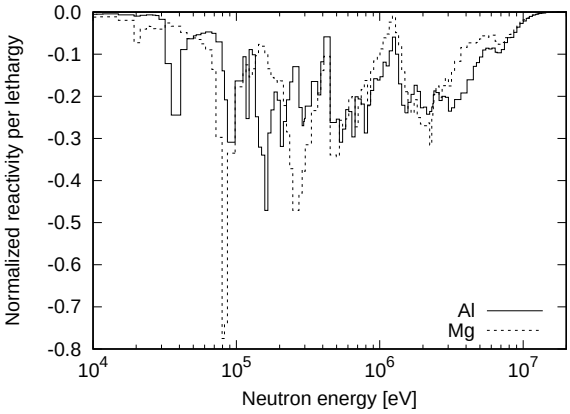

Figure 12 Energy break-down of the Al and Mg sample reactivity at SEG-6/45

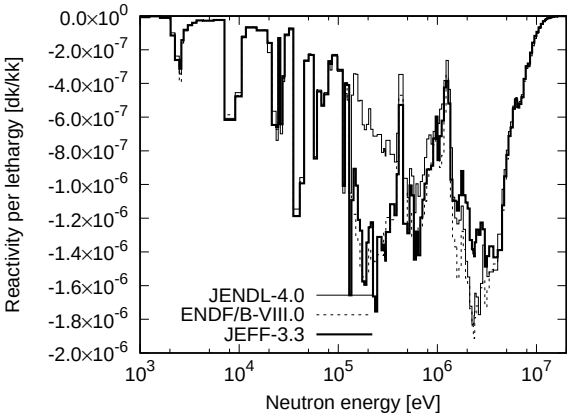

Figure 13 Energy break-down of the Mn sample reactivity at SEG-6/45

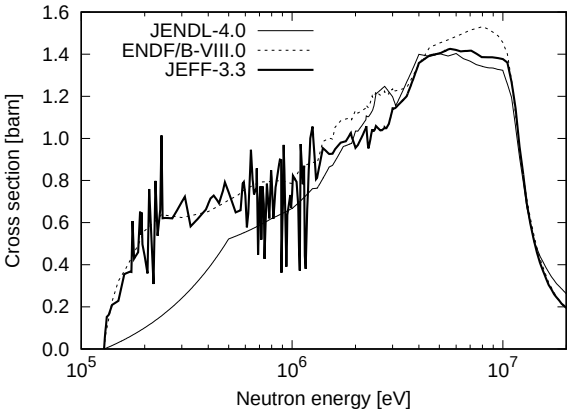

Figure 14 Inelastic scattering cross section of Mn-55

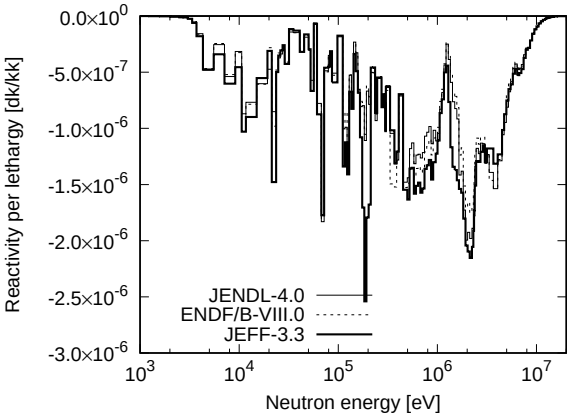

Figure 15 Energy break-down of the V sample reactivity at SEG-6/45

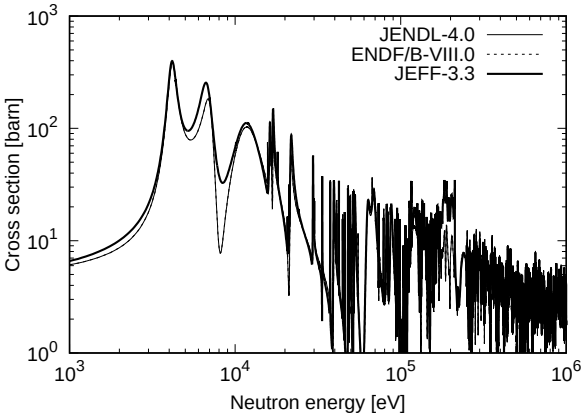

Figure 16 Elastic scattering cross section of V-51

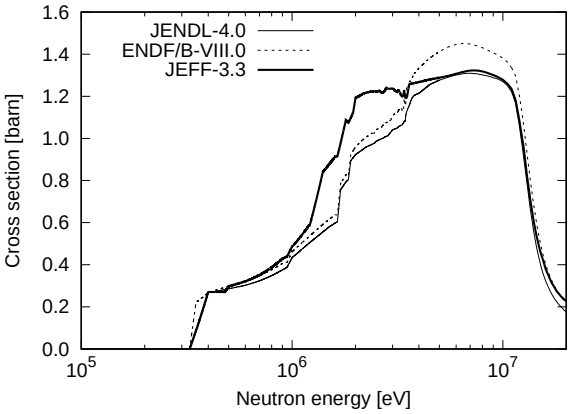

Figure 17 Inelastic scattering cross section of V-51